KSCE Journal of Civil Engineering (2020) 24(3):879-889
DOI 10.1007/s12205-020-1035-9

pISSN 1226-7988, eISSN 1976-3808
www.springer.com/12205

Structural Engineering

Effect of Horizontal Restraints on Progressive Collapse Resistance of Precast Concrete Beam-Column Framed Substructures

Feiliang Wang[a], **Jian Yang**[a,b], **and Sandeep Shah**[a]

[a]*School of Naval Architecture, Ocean and Civil Engineering, Shanghai Jiao Tong University, Shanghai 200240, China*
[b]*School of Civil Engineering, University of Birmingham, Birmingham B15 2TT, UK*

ARTICLE HISTORY

Received 12 June 2019
Revised 1st 30 September 2019
Revised 2nd 29 October 2019
Accepted 8 January 2020
Published Online 14 February 2020

KEYWORDS

Progressive collapse
Precast concrete frame
Horizontal restraints
Experimental study
Numerical simulation

ABSTRACT

The aim of this study is to reveal the effect of horizontal restraints on the progressive collapse behaviour of precast concrete (PC) framed substructures. To this end, two one-thirds-scale 2-storey 2-span beam-column sub-frames with varying horizontal restraint conditions have been experimentally investigated. A nonlinear finite element (FE) model based on ABAQUS package was established and validated against failure modes and load-carrying capacity recorded in the test. Parametric studies were conducted using the FE simulation approach to investigate the effect of key design variables on the performance of the PC sub-frames. It was found that the failure of the PC beam-column assemblies was dominated by pull-out of anchorage bars on side joints and the load-carrying capacity of the PC sub-frames were considerably affected by horizontal restraints.

1. Introduction

Structural progressive collapse has attracted numerous attentions since the disproportionate collapse of Ronan point happened in 1968. Soon after that, conceptual guidelines for progressive collapse design were initially introduced by UK Building Regulations (Approved document A, 2010) on 1970 and followed by more detailed provisions proposed in European (EN 1991-1-7, 2006) and US codes (GSA, 2003; DoD, 2005). For reinforced concrete (RC) structures, the understanding of structural progressive collapse was largely extended by analytical, experimental and numerical investigations in the last few decades. It has been concluded that compressive arch action (CAA) and catenary action can lead to a significant enhancement in the structural progressive collapse resistance (Yu and Tan, 2013), and it was observed that the failure of the RC frame was controlled by the rupture of the reinforcing steel bars in the floor beams (Yi et al., 2008). Based on the laboratory tests, it was indicated that the increase of transverse reinforcement ratio of the beam can improve the effectiveness of the CAA and result in a higher ultimate capacity of the RC frame (Qian and Li, 2013). By using a numerical approach, Elsanadedy et al. (2019) developed a nonlinear FE model for special moment-resisting RC frames under column-loss scenarios. In the model, bond-slip effects at the rebar-concrete interface were considered and the FE approach showed a good correlation with the test results. Analytical approach has shown that the sequence of column removal had a major effect on progressive collapse (Fascetti et al., 2015) and the provision of additional longitudinal reinforcement bars in the mid-layer of reinforced concrete beams was evidence in improving the ductility and load-resisting capacity of concrete beams subjected to a column removal scenario (Alogla et al., 2016). Moreover, it was concluded that the membrane action of slabs has a significant effect on progressive collapse resistance, and ignored the contribution from slabs led to incorrect simulation and uneconomic design outcome (Elshaer et al., 2017).

For PC frames, which are composed of discontinuous prefabricated components, the connections between precast elements are quite critical to secure the continuity and robustness of the structure (Nimse et al., 2014; Guan et al., 2019). By investigating a full-scale two-bay one-storey precast moment-resisting frame under the column-removal scenario, Main et al.

CORRESPONDENCE Jian Yang j.yang.1@sjtu.edu.cn School of Naval Architecture, Ocean and Civil Engineering, Shanghai Jiao Tong University, Shanghai 200240, China; School of Civil Engineering, University of Birmingham, Birmingham B15 2TT, UK

(2014) observed that premature non-ductile fracture of the lower anchorage bars has occurred in the vicinity of the welded connection to the centre column and the welded joints showed poor performance under column loss scenario in the middle. Kang and Tan (2015) concluded that PC connection can exhibit almost similar behaviour to monolithic RC connection by using 90° bend and lap splice of bottom reinforcement. Tohidi and Baniotopoulos (2017) and Tohidi et al. (2014) investigated the effect of the floor-to-floor joint on the catenary behaviour of precast concrete slab system, and found that for the ties designed with inadequate embedment length, the slip and resulting large deflection would effectively trigger the catenary action. Regarding numerical studies, Elsanadedy et al. (2017) developed a nonlinear FE model to predict the performance of precast non-prestressed RC beam-column subassemblies under the column-removal scenario. The validated FE modelling was further extended to study the progressive collapse potential of revised precast connections. High potential for the progressive collapse was found in prevalent beam-column connections in precast buildings. To this end, some rehabilitation techniques were proposed to strengthen beam-column connections in the event of sudden column-loss scenario (Almusallam et al., 2018; Al-Salloum et al., 2018).

To the author's best knowledge, the effect of horizontal restraints on PC frames has not been studied thoroughly. By using experimental and numerical approaches, this paper investigates the progressive collapse performance of PC beam-column framed substructures under varying horizontal restraint conditions. The CAA, catenary action and crack pattern developed in the specimens were examined. Numerical models presented were validated against experimental results. Besides, parametric studies were conducted to reveal the effect of concrete compressive strength, beam reinforcement ratio and horizontal restraint location on the load-carrying capacity of the PC sub-frame.

2. Experimental Studies

2.1 Specimen Designs and Test Setup

In the test, two 2-span 2-storey 1/3 scaled PC beam-column framed substructure specimens were prepared; one was doubly restrained in the horizontal direction and another was singly restrained which was without lower horizontal restraints (as marked in Fig. 1(a)). The floor height of the specimens was 1 m

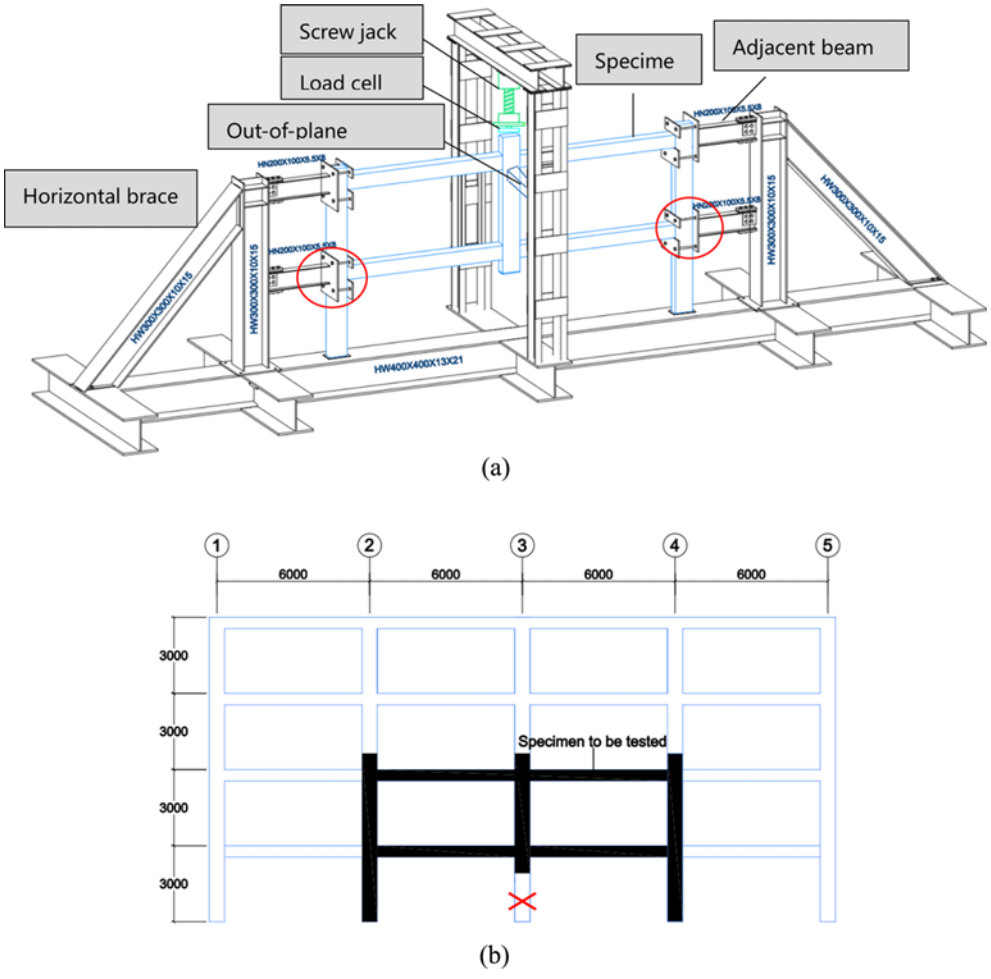

Fig. 1. Test Setup and Prototype Building of Doubly Restrained Specimen: (a) Test Setup, (b) Prototype Building (Note: Lower restraints marked in red circles were removed in the test for singly restrained specimen.)

Table 1. Comparison of Geometric Properties and Reinforcement Detailings between Prototype Building and the Scaled Specimens

Item	Beam			Column		
	Dimension (mm)	Longitudinal reinforcement	Stirrups	Dimension (mm)	Longitudinal reinforcement	Stirrups
Prototype buliding	450 × 300	3ϕ25; 3ϕ25	ϕ8@100/200	600 × 600	16ϕ28	ϕ10@100
Scaled specimen	150 × 100	2ϕ10; 2ϕ10	ϕ6@50/100	200 × 200	12ϕ12	ϕ8@50

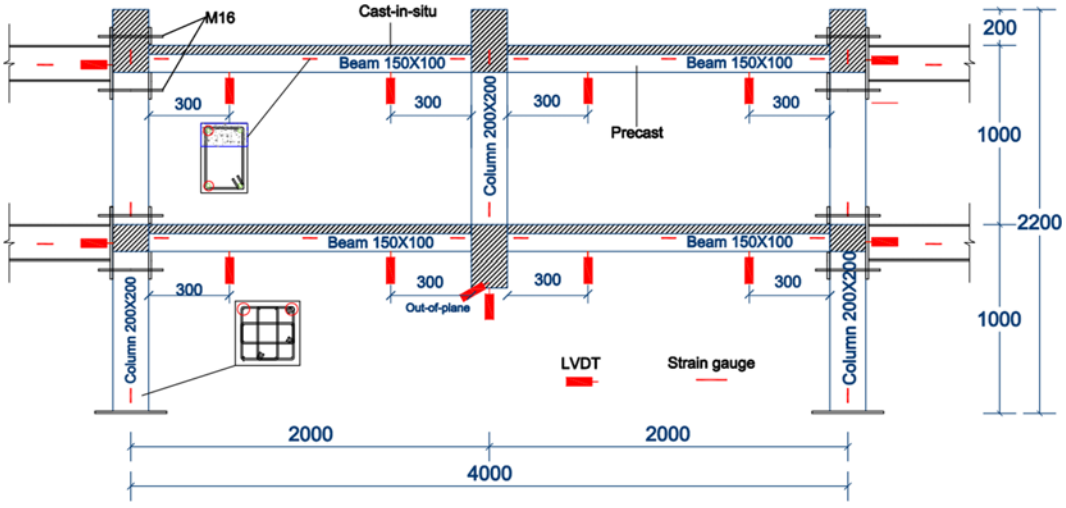

Fig. 2. Test Instrumentation in Doubly Restrained Specimen

and the span length was 2 m. From the figure, it can be seen that the lower central column of the specimen was removed in order to trigger the progressive collapse of the sub-assemblage. The specimen represents part of an actual 4-story framed building, as shown in Fig. 1(b). Comparisons of geometric properties and reinforcement detailing between the prototype building and the scaled specimen are shown in Table 1. The specimens were placed on a strong reaction frame with pin supports at each column end. A 250 kN screw jack installed at the top of the central column was employed to apply downward load. The load was applied under displacement control at the rate of 2 mm/min and the load data was recorded by a load cell placed on the top surface of the central column. The displacement of the specimens was measured by 14 Linear Variable Differential Transformers (LVDTs), as shown in Fig. 2. Strain gauges mounted on reinforcing bars and steel beams were used to monitor the strain distribution at each critical section.

Connection detailing of the specimen was designed by following Chinese specification (GBT-51231, 2016), as depicted in Figs. 3(a) and 3(b). It has to be pointed out that the longitudinal reinforcing rebars of the beam were continually installed and anchored to the side column with endplates (Fig. 3(c)). For the beams and columns of the specimens, the diameter of the longitudinal bars ranged from 10 mm to 12 mm and diameter of stirrups ranged from 6 mm to 8 mm, while 10 mm/12 mm bars had a nominal yield strength of 375 MPa and 6 mm/8 mm bars had a nominal yield strength of 235 MPa. According to coupon tests, the concrete used for the specimen was found to have a nominal cubic compressive strength of 27 MPa. Top and bottom reinforcement ratio of the beam was 1.3% (2C10) with the concrete cover of 20 mm, and the reinforcement ratio can be calculated by $\rho = A_s/bd$, in which b and d are the width and the effective depth of beam section. Horizontal restraints to the specimens were provided by strong steel braces at both ends. The braces were connected to the side columns via four adjacent beams (with the section of HN 200 × 100 × 5.5 × 8 mm) with twelve end plates (thickness of 12 mm) and sixteen M16 steel bars (with a diameter of 16 mm and yield strength of 640 MPa), as shown in Fig. 3(d). The out-of-plane movement of the specimen after casting to the experimental set-up was limited by restraining laterally via a hydraulic jack.

2.2 Test Results

An overall progressive collapse behaviour of the PC specimens can be seen in the relationships between the applied load against middle joint displacement (MJD) and axial horizontal reaction force against MJD. It can be seen that two curves have a similar developing tendency, and each curve has three stages before failure: elastic stage (OA/O'A'), transition stage (AB/A'B') and catenary stage (BC/B'C'). In the first stage, the curve is elastically ascending. As the load increases, the specimen enters into the second stage. During the stage, the compressive force can be noticed in the adjacent beam due to CAA, as shown in Fig. 5, and additional flexural strength was accommodated in the frame. The specimens experienced a transition from beam mechanism to catenary action when plastic hinges formed on the beams.

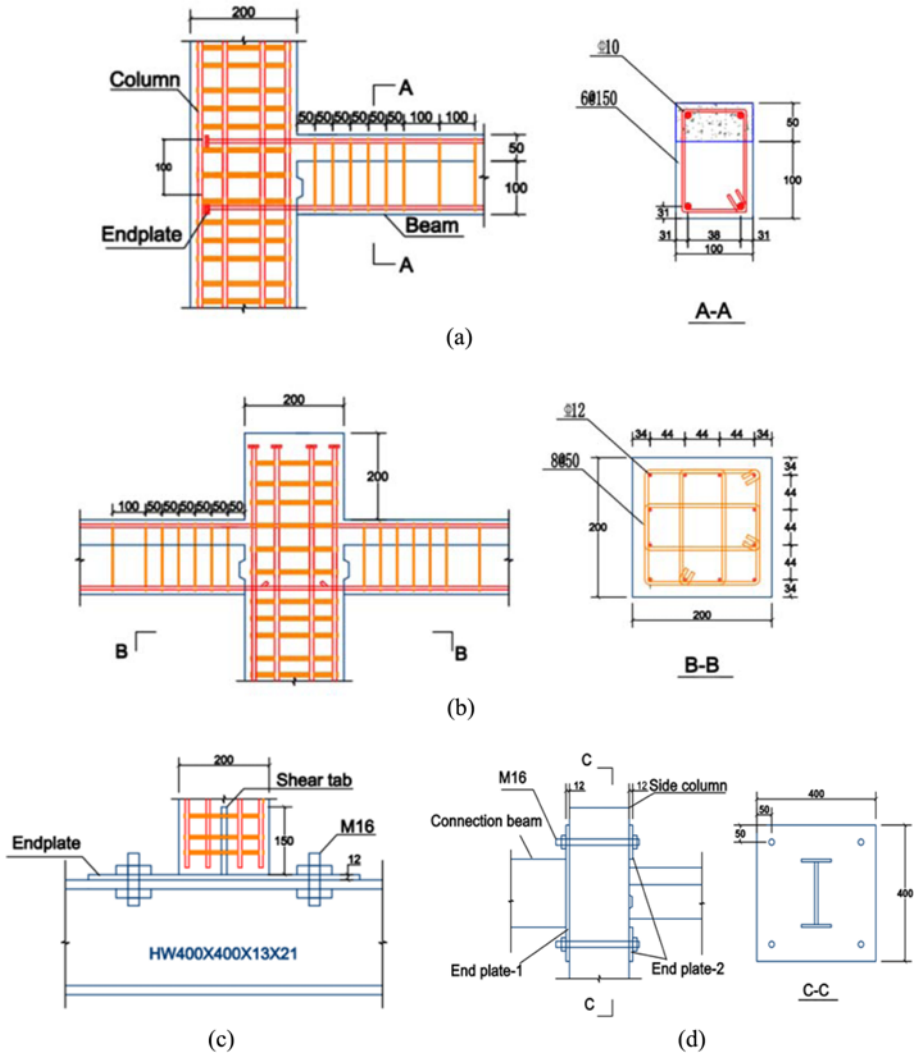

Fig. 3. Geometric Dimensions and Connection Details of the Specimen: (a) Side Column-Beam Connection, (b) Middle Column-Beam Connection, (c) Column End Connection, (d) Horizontal Restraint for the Side Column

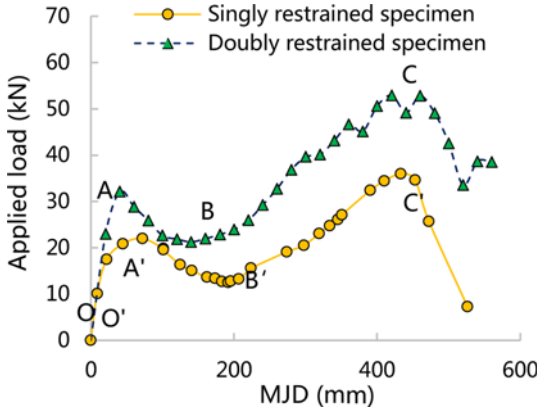

Fig. 4. Applied Force versus MJD

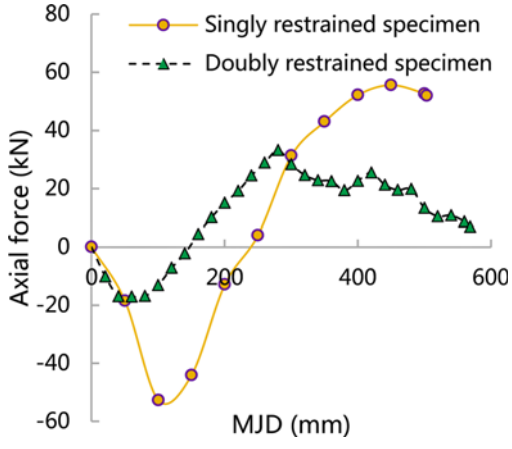

Fig. 5. Horizontal Restraint Reaction Force versus MJD

Meanwhile, the applied load against MJD curves experience a sagging tendency and axial force in the beam changes from compression to tension, which indicates the commencement of the catenary action. The applied load increased again during the catenary stage and the specimen associated with large-deformation behaviour. At the moment, the resistance of the frame was mainly undertaken by anchorage bars at the side joints and the

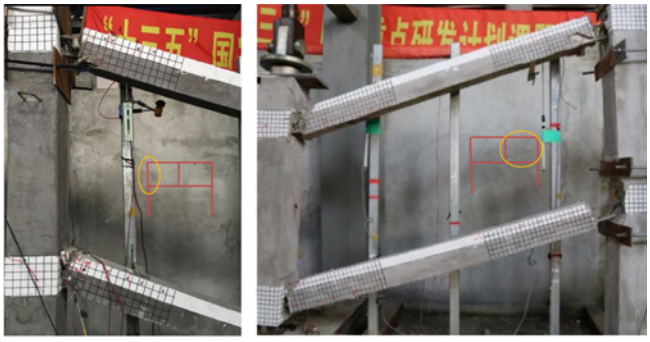

Fig. 6. Photograph of Specimen Behaviours at the End of the Test: (a) Singly Restrained Specimen, (b) Doubly Restrained Specimen

bars were observed being pull-out gradually. Then, the failure of the specimens occurred after point C/C'. The endplates of the anchorage bars were ruptured and the bars were totally pulled out from the side columns (Fig. 6). A considerable increase (46.7%) in the ultimate capacity was noticed in the specimen with doubly horizontal restraints. Good ductile behaviour was observed in both singly and doubly restrained specimens with the MJD of 433 and 460 mm respectively at the ultimate load. For the singly restrained specimen, the failure was controlled by pull-out of the upper storey anchorage bars; for the doubly restrained specimen, the failure was governed by both upper and lower storey anchorage, this is the reason that the latter has greater had greater displacements before failure.

Figure 7 depicts crack development at different stages of loading for the left side joint and right central joint of the singly restrained specimen. At the initial stage, flexural cracks were uniformly distributed on both ends of the beam. Limited cracks were observed at the beam mid-span section during the stage. Then, more cracks were observed at tension areas of the central joint and the side joint and a reduction of the CAA capacity can be noted. Severe concrete crushing and spalling can be noticed when point B is reached. Existing cracks continued to expand and open up in the catenary stage and stopped at the location of the neutral axis of the beam. At the final stage, the failure of the specimen occurred by the rupturing of the endplate and the pulling out of the anchorage bars. Meanwhile, the beam-column interfaces were separated, which can be attributed to an insufficient bond between cast-in-situ concrete and precast concrete. It is worth noting that for RC frames, cracks after flexural action uniformly developed throughout the beam length (Alogla et al., 2016), but in PC frames, cracks mainly concentrated on the beam-column interfaces. The key results and observations in the test are summarized in Table 2.

The deflection profile of the beam was described by the LDVT that captured vertical displacement at specific points along the length of the beam at different critical load steps, as shown in Fig. 8. It can be inspected that symmetry of the beam deflections at both sides of the specimen was maintained during the test. The initial deflection of the beam is not significant until the maximum compression capacity was achieved, then, a substantially increasing displacement has been noted during the

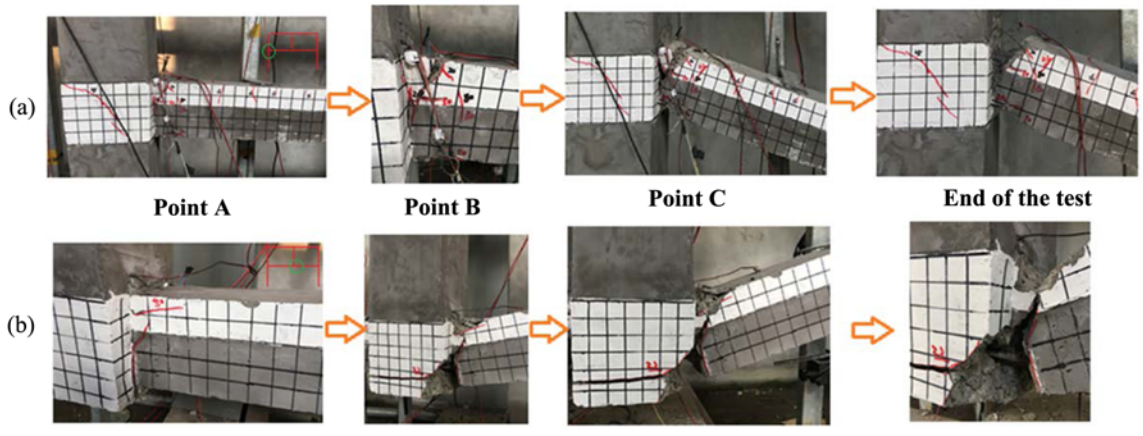

Fig. 7. Crack Pattern of the Singly Restrained Specimen: (a) Left Side Joint, (b) Central Joint

Table 2. Summary of Test Results

Description	Singly restrained specimen		Doubly restrained specimen		Observations
	Load (kN)	MJD (mm)	Load (kN)	MJD (mm)	
Elastic limit (A/A')	17.5	22.1	23.0	20.7	Flexural cracks are occurring on the beam ends
Start of catenary action (B/B')	15.6	223.6	22.0	160.3	Cracks are expanding and beam-column interfaces are separating
Max. load-carrying capacity (C/C')	36.0	433.0	52.8	460.0	End plates are ruptured and the anchorage bars are pulling out in the side joints

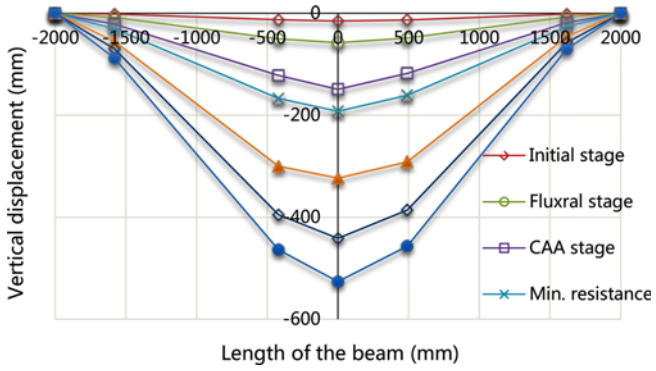

Fig. 8. Beam Deflection Profile of the Singly Restrained Specimen

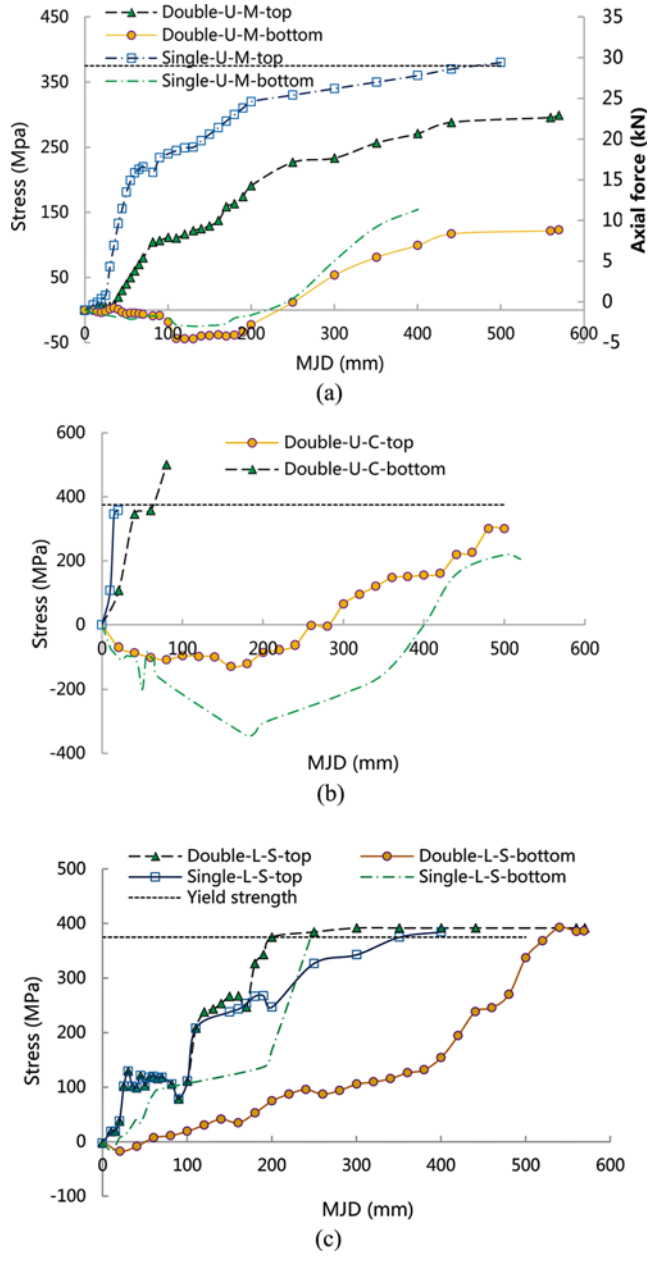

Fig. 9. Stress Development of Reinforcing Bars: (a) Mid-Span Section: (b) Central Joint, (c) Side Joint

catenary stage.

The performance of the specimens can be evidenced by the stress development of beam longitudinal reinforcing bars. Fig. 9 shows the relationship between stress at the top (T) and bottom (B) reinforcing bars against MJD at different locations of the beam. In the figure, notations such as "single" and "double" represents singly restrained specimen and doubly restrained specimen, "U" and "L" refer to upper beam and lower beam, "M", "C" and "S" refer to mid-span section, central joint section and side joint section, respectively.

At the mid-span section, the stress development curves of the upper beam are comparable in both specimens. The tensile stress in the top bars of the singly restrained specimen was greater than that of the doubly restrained specimen, indicating the applied load was mainly undertaken by the upper beams in the singly restrained specimen. The stress in the bottom reinforcing bars is changed from compression to tension, which represents that compression was applied to the beam due to CAA. Both top and bottom bars are witnessed in contribution to the tension forces at the catenary action stage. The tensile stress of the bottom reinforcing bars at the central joint increases dramatically during the beam mechanism, meanwhile, compressive stress is initially found in the top bars and then changes to tensile stress after the maximum CAA capacity is achieved. Almost no compression is found in the bottom reinforcing bars at the side joint of the singly restrained specimen; this is because of CAA cannot be fully developed in the beam when horizontal restraint stiffness is insufficient.

3. Numerical Simulations

3.1 Finite Element Models

In addition to the experimental studies, finite element (FE) program ABAQUS (2013) was employed to develop numerical models replicating the aforementioned specimens. The FE model is illustrated in Fig. 10, noting that the model geometry and details were inconsistent with the tested specimens. Concrete components were simulated using solid element C3D8R (8-node linear brick, reduced integration, and hourglass control) whilst T3D2 (2-node linear 3-D truss) truss elements were adopted to mesh the reinforcing bars and stirrups. The reinforcement was embedded in the concrete and the effect of bond-slip was not considered in the model. As the contact condition was considered critical in the simulation of PC structures, the combined contact strategy was used as follows: beam-column interfaces between precast concrete and cast-in-situ concrete were simulated by surface-to-surface contact and "Tie" contact was applied to the rest interfaces. In the surface-to-surface contact, "hard" contact was applied to the normal direction to prevent press-penetration while friction contact was applied to the tangential direction with a friction coefficient of 0.8. The adopted mesh pattern was as follows: the basic mesh size was 40 mm with a refined mesh size of 20 mm applied around the beam-column joint. The friction coefficient and mesh size were selected by means of sensibility

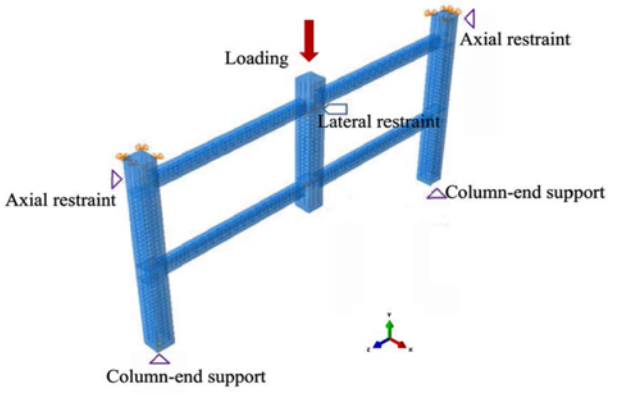

Fig. 10. Finite Element Model of the Singly Restrained Specimen

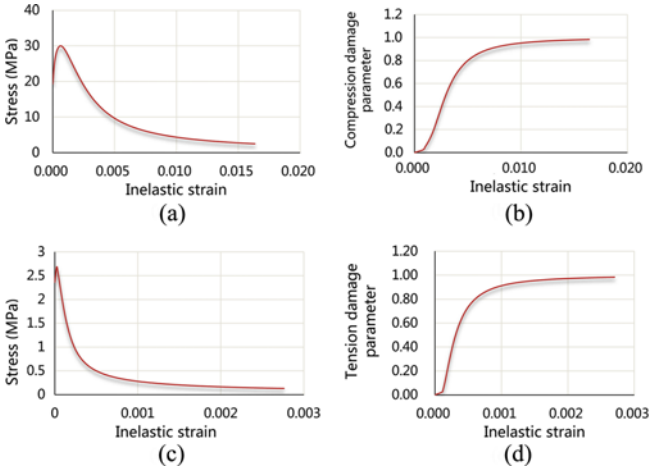

Fig. 11. CDP Properties in the FE Model: (a) Concrete Compressive Behaviour, (b) Concrete Compressive Damage Behaviour, (c) Concrete Tensile Behaviour, (d) Concrete Tensile Damage Behaviour

analysis.

The material property for the concrete was simulated by Concrete Damage Plasticity (CDP) behaviour which assumed tensile cracking and compressive crushing as a failure mechanism. The complete stress-strain compressive curve of concrete was derived using Popovics's model (Popovics, 1973) and the tensile curve based on the model presented by Belarbi et al. (1996). The details of the material properties of concrete are given in Fig. 11. For the longitudinal reinforcing bars and stirrups, the material properties were defined as bilinear stress-strain curves with the yield strength of 375 MPa and 235 MPa and rupture strain of 0.16 and 0.2, respectively. The concentrated displacement load was applied to a reference point which coupled with the top surface of the central column. Horizontal restraints were applied to both sides of the specimen, and out-of-plane movement of the specimen was restrained by lateral restraint and pinned supports were applied to the column ends to fix all translations. The numerical analysis was performed using the nonlinear dynamic explicit integration method, which was assumed can accommodate damage behaviours and was beneficial in avoiding convergence problems.

3.2 Model Validations

In order to verify the developed FE model, three criteria from the experimental and numerical were compared. They were applied load versus MJD, failure modes and the stress development in beam longitudinal reinforcing bars. Fig. 12 compares the experimentally recorded load-MJD curves and those obtained from the numerical simulation. The numerical response gave acceptable predictions for the resistance of the specimens, as the FEM/Test ratio of the first peak load and ultimate load are 1.00 and 0.88 for the singly restrained specimen and 0.98 and 1.05 for the doubly restrained specimen. The initial stiffness of the FE model was slightly higher than that of the test, which is due to that there were micro-cracks in the practical specimens as a result of shrinkage during drying, handling and transporting process, however, the micro-cracks were not simulated in the FE model. The discrepancy of the resistance between curves may be attributed to that the anchorage bars have yielded in the model rather than pull-out failure in the test. This can be concluded that the developed modelling method, which ignored the bond-slip effect between concrete and reinforcement, is more efficient in simulating bar fracture behaviour rather than pull-out behaviour. From Fig. 13, it can be seen that the failure modes are similar between two methods, indicating that the applied CDP material property and interactions are able to capture the cracking damage behaviour of the concrete under progressive collapse scenario.

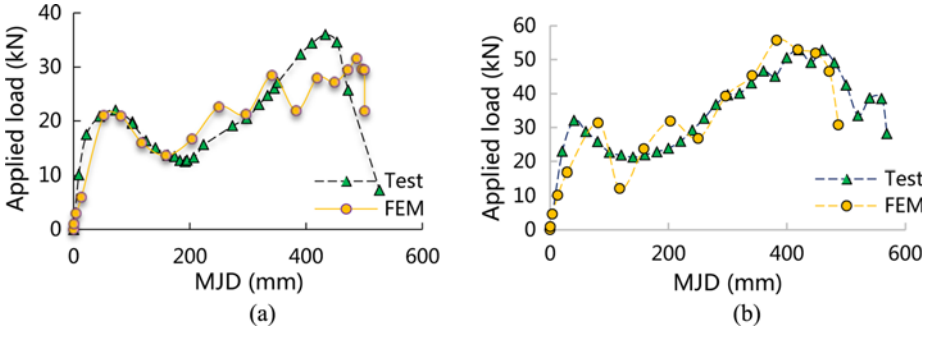

Fig. 12. Comparison of Applied Load vs. MJD Curves: (a) Singly Restrained Specimen, (b) Doubly Restrained Specimen

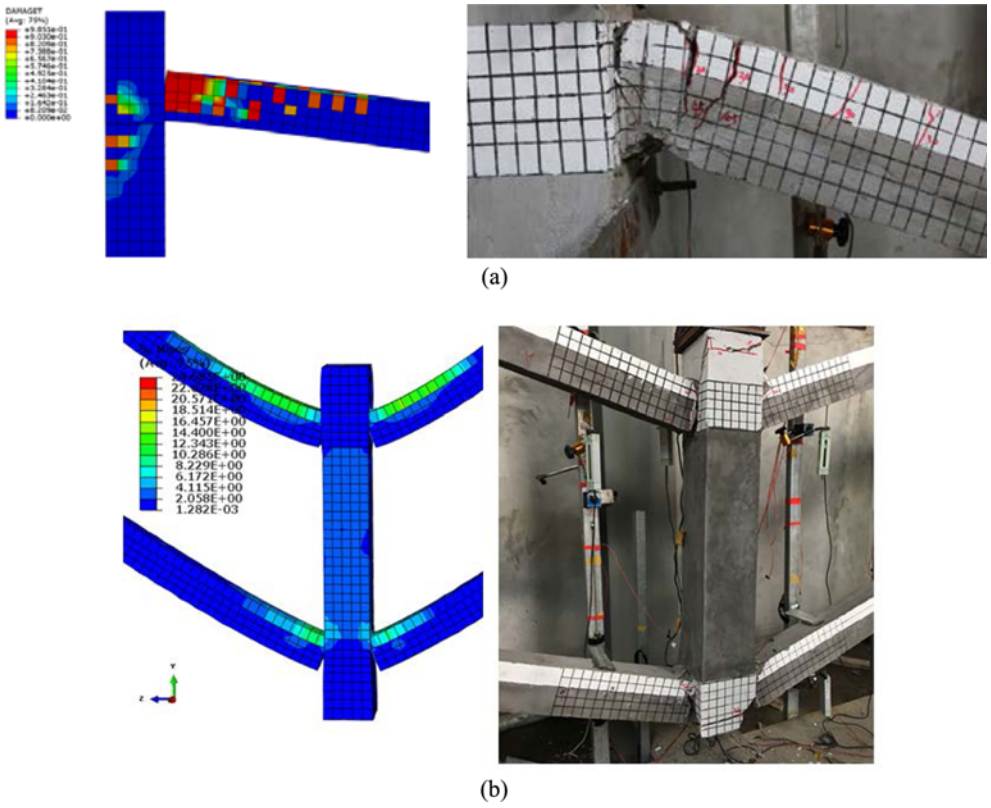

Fig. 13. Failure Modes of the Singly Restrained Specimen: (a) At the Side Joint, (b) At the Central Joint

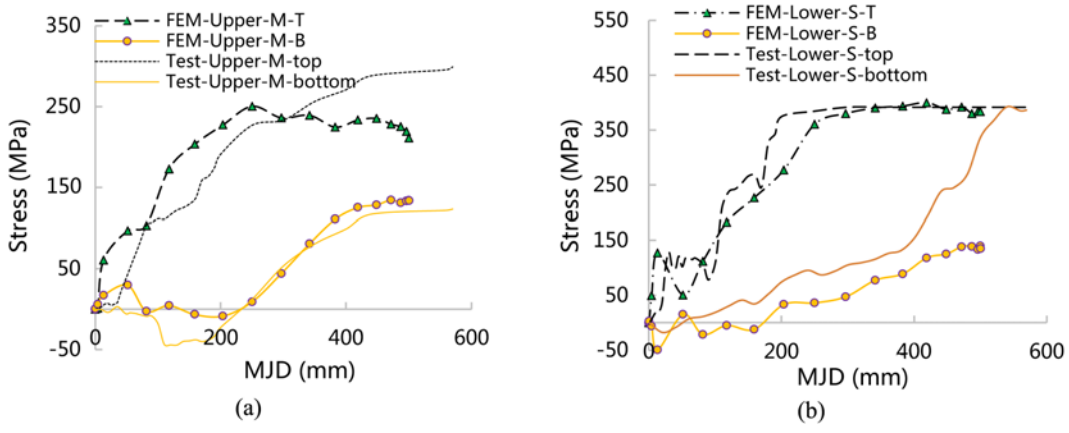

Fig. 14. Stress Development of the Reinforcing Bars in the Beam: (a) In the Upper Beam, (b) In the Lower Beam

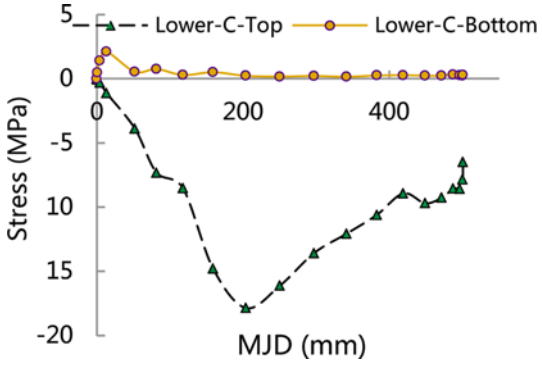

Fig. 15. Stress Development of the Concrete

From Fig. 14, stress development of reinforcing bars by FEM has a good agreement to the test results. The development of concrete stress is displayed in Fig. 15. It shows that bottom concrete of the beam at the central joint reaches tensile strength when MJD is about 13 mm and this part is stop working in the catenary stage. The stress of the top concrete at central joint attains maximum compressive capacity when MJD reaches 200 mm. Meanwhile, plastic hinges formed in the beam (Fig. 16) and catenary action was initiated in the frame.

3.3 Parametric Studies

A series of parametric studies were conducted based on the

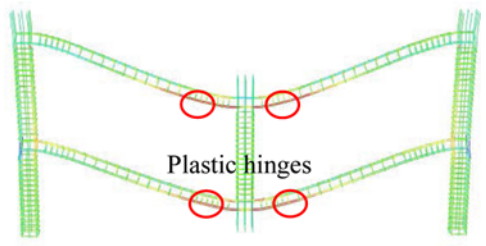

Fig. 16. Stress Contour of the Reinforcing Beams (MJD = 200 mm)

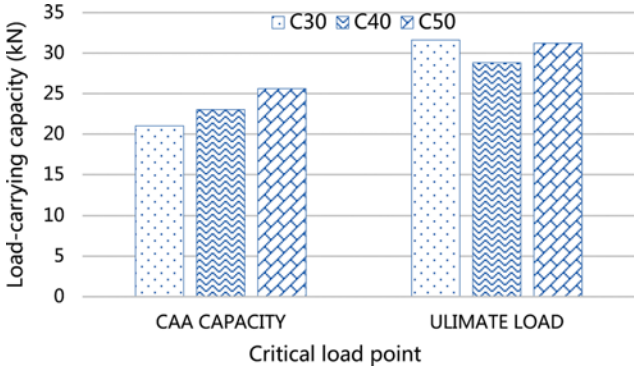

Fig. 17. Effect of Concrete Compressive Strength

validated FE approach to give insight into the influence of the concrete compressive strength, reinforcement ratio and horizontal restraint location on progressive collapse resistance of the PC sub-frame. It is noteworthy that only one variable was changed at a time during the analysis.

3.3.1 Concrete Compressive Strength

Comparison of load-carrying capacity with concrete strength from 30 MPa to 50 MPa is visible in Fig. 17. It suggests that as the concrete compressive strength increases, the load-carrying capacity during CAA increases as expected. The capacity rises by 9.5% and 11.3% when increasing concrete compressive strength from 30 MPa to 40 MPa and from 40 MPa to 50 MPa, respectively. The increase in the ultimate capacity is not significant with improving concrete strength as the resistance is mainly provided by reinforcement during the catenary stage.

3.3.2 Reinforcement Ratio

The effect of beam longitudinal reinforcement ratio on the load-resistance capacity is shown in Fig. 18. In the study, top reinforcement ratio in the beam is increased from 0.85% to 1.9% while the bottom reinforcement ratio remains at 1.3%; and the beam bottom reinforcement ratio increases from 0.85% to 1.9% when the beam top reinforcement ratio is levelling off at 0.85%.

The result shows that increase in beam top longitudinal reinforcement ratio i.e., from T0.85/B1.3 to T1.9/B1.3 increases the CAA capacity by 24% (from 16.2 kN to 20.1 kN) and enhances ultimate capacity by 10% (from 27.6 kN to 30.4 kN). Similarly, the increase in beam bottom longitudinal ratio i.e., from T0.85/B0.85 to T0.85/B1.9 increases the CAA capacity by 13% and enhances the catenary action resistance by 79%. Indicating that the improvement of the load-carrying capacity induced by increasing the bottom reinforcement ratio is more significant than increasing top reinforcement ratio.

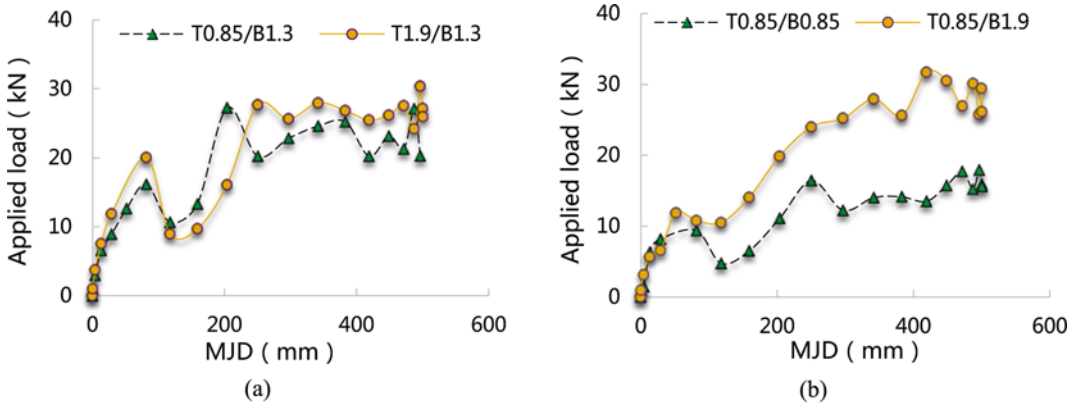

Fig. 18. Effect of Beam Longitudinal Reinforcement Ratio: (a) Various Top Reinforcement Ratio, (b) Various Bottom Reinforcement Ratio

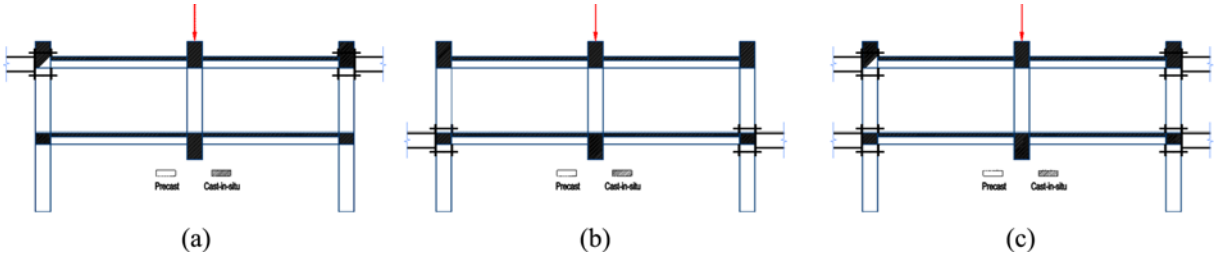

Fig. 19. Plot of Specimens with Various Restraint Location: (a) Lower Restraints Released (LR), (b) Upper Restraints Released (UR), (c) Doubly Restrained (DR)

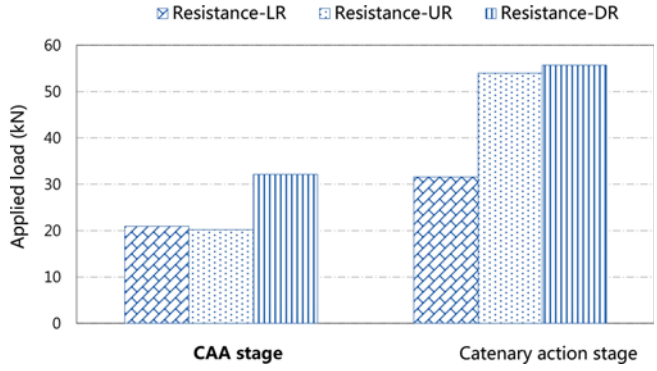

Fig. 20. Effect of Horizontal Restraint Location

3.3.3 Horizontal Restraints Location

In order to further reveal the effect of restraint, three models with varying restraint scenarios, namely LR, UR and DR (Fig. 19), were compared in FEM. The maximum resistances at CAA and catenary action stage of each model are illustrated in Fig. 20. It can be seen that the CAA maximum resistance is similar between UR and LR specimen, while the former has a considerably greater ultimate resistance (by 70.9%) in the catenary stage. This is because that inward movement of the side column in the UR specimen will introduce an extra flexural to the lower beam-side column joint and reduce the tension at the joint. This also signifies the importance of horizontal restraints at each storey beam levels for the successful development of catenary action in the progressive collapse scenario.

4. Conclusions

In this paper, the effect of horizontal restraint on the structural behaviour of two 2-storey 2-span 1/3 scaled 2D- PC frame under central column-removal scenario has been investigated experimentally and numerically. The following conclusions can be drawn based on the test results and numerical findings:

1. From the failure pattern of the specimen, it was revealed that the cracks were mainly concentrated on the interfaces of beam-column joints, which was due to an insufficient bond between cast-in-situ concrete and precast concrete. The failure of the substructures was dominated by pull-out of the anchorage reinforcing bars at the side joint.
2. A significant effect of horizontal restraints was observed by comparing the load-carrying capacity between the singly restrained specimen and the doubly restrained specimen. The additional two lower restraints have resulted in an increase of 46.7% in the ultimate capacity.
3. The comparison between experimental and numerical results indicates that the developed simulation approaches i.e., CDP model and interaction strategy are capable of simulating the resistance and cracking pattern of the PC frame specimen.
4 It is evident that the introduction of increasing beam longitudinal reinforcement ratio in the parametric study has a beneficial effect. The increase in beam bottom reinforcement ratio yields a better scheme to beam top reinforcement ratio in the successful development of catenary action (CA).
5. The horizontal restraint location was found has considerable influence on the ultimate resistance of the sub-frame, and the UR specimen leads to an increase by 70.9% when compared with LR specimen.

Acknowledgements

The authors are grateful for the financial support of the National Science and Technology Major Project (2016YFC0701400) and China Postdoctoral Science Fund (17Z102060052).

ORCID

Feiliang Wang https://orcid.org/0000-0002-1630-3204

References

ABAQUS (2013) Analysis user's manual, version 6.13. SIMULIA, Province, RI, USA

Almusallam TH, Elsanadedy HM, Al-Salloum YA, Siddiqui NA, Iqbal RA (2018) Experimental investigation on vulnerability of precast RC beam-column joints to progressive collapse. *KSCE Journal of Civil Engineering* 22(10):3995-4010, DOI: 10.1007/s12205-018-1518-0

Alogla K, Weekes L, Augusthus-Nelson L (2016) A new mitigation scheme to resist progressive collapse of RC structures. *Construction and Building Materials* 125:533-545, DOI: 10.1016/j.conbuildmat.2016.08.084

Al-Salloum YA, Alrubaidi MA, Elsanadedy HM, Almusallam TH, Iqbal RA (2018) Strengthening of precast RC beam-column connections for progressive collapse mitigation using bolted steel plates. *Engineering Structures* 161(4):146-160, DOI: 10.1016/j.engstruct.2018.02.009

Approved document A (2010) The building regulation, A3: Disproportional collapse. UK HM Government, London, UK

Belarbi A, Zhang LX, Hsu TTC (1996) Constitutive laws of reinforced concrete membrane elements. Eleventh world conference of earthquake, June 23-28, Acapulco, Mexico

DoD (2005) Design of buildings to resist progressive collapse. UFC 4-023-03, Department of Defense, Unified Facilities Criteria (UFC)

Elsanadedy H, Almusallam T, Al-Salloum Y, Abbas H (2017) Investigation of precast RC beam-column assemblies under column-loss scenario. *Construction and Building Materials* 142:552-571, DOI: 10.1016/j.conbuildmat.2017.03.120

Elsanadedy HM, Al-Salloum YA, Almusallam TH, Ngo T, Abbas H (2019) Assessment of progressive collapse potential of special moment resisting RC frames-Experimental and FE study. *Engineering Failure Analysis* 105:896-918, DOI: 10.1016/j.engfailanal.2019.07.045

Elshaer A, Mostafa H, Salem H (2017) Progressive collapse assessment of multistory reinforced concrete structures subjected to seismic actions. *KSCE Journal of Civil Engineering* 21(1):184-194, DOI: 10.1007/s12205-016-0493-6

EN 1991-1-7 (2006) Actions on structures, Part 1-7: General actions - accidental actions. EN 1991-1-7, European Committee for Standardization, Brussels, Belgium

Fascetti A, Kunnath SK, Nisticò N (2015) Robustness evaluation of RC

frame buildings to progressive collapse. *Engineering Structures* 86:242-249, DOI: 10.1016/j.engstruct.2015.01.008

GBT-51231 (2016) Technical standard for assembled buildings with concrete structure. China National Standard, The Standards Press of China, Beijing, China

GSA (2003) Progressive collapse analysis and design guidelines for federal office buildings and major modernization projects. General Services Administration, Washinton (DC) Office of Chief Architect, Washington, DC, USA

Guan DZ, Guo ZX, Jiang C, Yang S, Yang H (2019) Experimental evaluation of precast concrete beam-column connections with high-strength steel rebars. *KSCE Journal of Civil Engineering* 23(1):238-250, DOI: 10.1007/s12205-018-1807-7

Kang SB, Tan KH (2015) Behaviour of PC beam-column sub-assemblages subject to column removal. *Engineering Structures* 93:85-96, DOI: 10.1016/j.engstruct.2015.03.027

Main JA, Bao YH, Lew HS, Sadek F (2014) Robustness of precast concrete frames: Experimental and computational studies. Structures congress 2014, April 3-5, Boston, MA, USA, DOI: 10.1061/9780784413357.194

Nimse RB, Joshi DD, Patel PV (2014) Behavior of wet precast beam column connections under progressive collapse scenario: An experimental study. *International Journal of Advanced Structural Engineering* 6:149-159, DOI: 10.1007/s40091-014-0072-3

Popovics S (1973) A numerical approach to the complete stress-strain curve of concrete. *Cement and Concrete Research* 3:583-599, DOI: 10.1016/0008-8846(73)90096-3

Qian K, Li B (2013) Performance of three-dimensional reinforced concrete beam-column substructures under loss of a corner column scenario. *Journal of Structural Engineering* 139:584-594, DOI: 10.1061/(ASCE)ST.1943-541X.0000630

Tohidi M, Baniotopoulos C (2017) Effect of floor joint design on catenary actions of precast floor slab system. *Engineering Structures* 152:247-288, DOI: 10.1016/j.engstruct.2017.09.017

Tohidi M, Yang J, Baniotopoulos C (2014) Numerical evaluations of codies design methods for progressive collapse resistance of precast concrete cross wall structrues. *Engineering Structures* 76:177-186, DOI: 10.1016/j.engstruct.2014.06.034

Yi WJ, He QF, Xiao Y, Kunnath SK (2008) Experimental study on progressive collapse-resistant behavior of reinforced concrete frame structures. *ACI Structural Journal* 105(4):433-439, DOI: 10.14359/19857

Yu J, Tan KH (2013) Experimental and numerical investigation on progressive collapse resistance of reinforced concrete beam column sub-assemblages. *Engineering Structures* 55:90-106, DOI: 10.1016/j.engstruct.2011.08.040